THE UNIVERSITY of EDINBURGH

Edinburgh Research Explorer

Effect of Poly(ethylene oxide) Molecular Weight on the Pinning and Pillar Formation of Evaporating Sessile Droplets

Citation for published version:
Mamalis, D, Koutsos, V, Sefiane, K, Kagkoura, A, Kalloudis, M & Shanahan, MER 2015, 'Effect of Poly(ethylene oxide) Molecular Weight on the Pinning and Pillar Formation of Evaporating Sessile Droplets: The Role of the Interface', *Langmuir*, vol. 31, no. 21, pp. 5908-5918. https://doi.org/10.1021/la504905y

Digital Object Identifier (DOI):
10.1021/la504905y

Link:
Link to publication record in Edinburgh Research Explorer

Document Version:
Peer reviewed version

Published In:
Langmuir

General rights
Copyright for the publications made accessible via the Edinburgh Research Explorer is retained by the author(s) and / or other copyright owners and it is a condition of accessing these publications that users recognise and abide by the legal requirements associated with these rights.

Take down policy
The University of Edinburgh has made every reasonable effort to ensure that Edinburgh Research Explorer content complies with UK legislation. If you believe that the public display of this file breaches copyright please contact openaccess@ed.ac.uk providing details, and we will remove access to the work immediately and investigate your claim.

Download date: 05. May. 2023

Effect of poly(ethylene oxide) molecular weight on the pinning and pillar formation of evaporating sessile droplets: The role of the interface

Dimitrios Mamalis[†], Vasileios Koutsos[†,*], Khellil Sefiane[†], Antonia Kagkoura[†], Michail Kalloudis[†¥], and Martin E. R. Shanahan[‡]

[†]Institute for Materials and Processes, School of Engineering, The University of Edinburgh, King's Buildings, Edinburgh EH9 3FB, United Kingdom

[‡]Univ. Bordeaux, I2M, UMR 5295, F-33400 Talence, France; CNRS, I2M, UMR 5295, F-33400 Talence, France; Arts et Metiers ParisTech, I2M, UMR 5295, F-33400 Talence, France

[¥]Impact Solutions, 16 Abbotisinch Road, Grangemouth FK3 9UX, United Kingdom

[*] To whom correspondence should be addressed: E-mail: vasileios.koutsos@ed.ac.uk; Tel.: +44 (0)131 650 8704; Fax: +44 (0)131 650 6551

ABSTRACT

We report on the drying process of sessile droplets of aqueous poly(ethylene oxide) (PEO) solutions studied by contact angle analysis. Liquid samples were prepared with the same initial concentration of four different molecular weights, M_w of PEO. Droplets with initial volumes between 1 μL and 5 μL were left to evaporate while temperature, pressure and relative humidity were kept constant. Residues were formed with either a disk-like puddle or a distinctive tall conical pillar shape. The latter occurred following a four-stage deposition process: pinned drying, during which the contact line is stationary; pseudo-dewetting, where the receding contact line is induced by precipitation; bootstrap building, during which the liquid droplet is lifted upon freshly-precipitated solid; and late drying. Contact angle analysis allowed us to monitor all stages during drying and consider transitions between stages for different molecular weights. We illustrate the mechanisms taking place during the crucial stages of pinning and depinning, revealing the effect of adhesion and contact line friction for high molecular weights and its influence on the final

morphology of the dried PEO solute. To this end, we performed PEO solution droplet evaporation on PEO and PTFE films demonstrating the importance of interfacial interaction phenomena. We show that the formation of disk-like puddles for high molecular weights on glass are associated with continuous droplet contact line pinning. This results from the strong adhesion due to the interdigitation of the loops and tails of a polymer layer (adsorbed on glass during evaporation) with the polymer gel network inside the droplet that forms as water evaporates.

Introduction

In recent years, there has been a rapid growth of interest in the technologically and scientifically important issue of the evaporation of liquid droplets. Particular attention has been paid to the evaporation mechanisms of pinned droplets of polymer solution. The growing scientific interest is related to advanced applications such as inkjet printing,[1, 2] evaporative cooling technologies.[3]

In the seminal work of Deegan *et al.*,[4] the phenomenon of 'coffee-stains' is circumstantially explained due to outward flow within the evaporating droplet. This outward flow is a combination of the increased evaporation rate at the droplet edge and the contact line pinning caused by solute deposition near the edge.[4] However, Shen *et al.* showed that for evaporating droplets, a lower limit of droplet size exists, for well-defined coffee ring formation to occur (above a concentration threshold).[5] This is owing to the competition between the liquid evaporation time and the particle diffusion time within the droplet. For suspended particles of size ~100 nm, the minimum diameter of the coffee ring structure is found to be ~10 μm. Small droplets will dry more quickly and the suspended particles will not have sufficient time to migrate to the contact line rim and

form the ring-stain.[5] Hu and Larson showed numerically that the ring formation behaviour can be suspended due to the presence of recirculating currents within the evaporating droplet caused by the thermal Marangoni flows.[6] They concluded that the coffee-ring phenomenon requires not only a pinned contact line, where particles adhere to the substrate, but also the suppression of the Marangoni effect which results from the surface-tension gradients due to the latent heat of evaporation.[6] The final morphology of the dried solute is not always a ring and depends on many experimental factors including: the solvent evaporation rate,[7] the shape of suspended particles,[8] interactions between solvent, solute, vapour and substrate,[9, 10] phase transitions within the droplet,[11, 12] self-assembly and organization as mediated by solvent dewetting,[13] and the contribution of any convective currents.[14]

Besides single component fluids and colloidal suspensions, drying experiments have been performed on droplets of polymer solutions. Polymers in solution can exist in many different phases depending on the crucial experimental parameters of concentration, c_0, and temperature, T. Pauchard *et al.*[12, 15] reported a number of complicated phenomena that arise as polymer solutions evaporate. In their study, during the evaporation process of dextran (a branched polysaccharide) solutions, the concentration at the droplet's edge increased due to the outward flux of the solution. This resulted in a phase change on the surface of the liquid droplet forming a glassy skin with spherical shape.[12, 15, 16, 17] Further evaporation and loss of water within the droplet led to the glassy cap deforming and buckling with various shapes. All these various complicated structures, including doughnut and sombrero-like deposits, depend on experimental conditions such as contact angle, relative humidity, temperature and concentration.[15]

The drying process of composite fluids such as polymer solutions involves a complex evolution which is related to a large number of microscopic phenomena such as solvent diffusion, transfer at the vapour/liquid/interface, concentration changes and phase transitions etc. In the present work, we examine the drying process of polyethylene oxide (PEO), one of the most extensively studied of all water-soluble synthetic polymers.[18, 19, 20, 21] It is a very common and widely used linear (non-branched) polymer[22, 23, 24, 25] and does not exhibit a glass transition (unlike dextran[15]) at high concentrations. PEO precipitates as a solid phase, usually in the form of semi-crystalline spherulites. It dissolves well in water, although at high concentrations or molecular weights polymer solutions can appear cloudy due to micron-sized clusters of undissolved polymer.[21] The origin of these clusters is still a point of speculation. Previous studies on drying droplets of PEO solution showed that the deposited solid structures could not be described by either the coffee ring-stain or skin buckling models, but required a four stage drying process: *pinned drying*; *pseudo-dewetting*; *boot-strap building*; and *solid contraction***.**[26, 27] Willmer *et al.* [26] proposed that the four stage drying process cannot be explained using a skin bulking model, as the surface area of the droplet is shown to increase during the growth stage. They concluded that a crucial mechanism during boot-strap stage takes place, in which the liquid droplet is lifted above the surface by the newly formed solid deposit, resulting in solid pillars.[26] Recent experimental work on the evaporation of PEO from Baldwin *et al.*[28] focused on a detailed description of each stage and proposed physical models to explain key aspects of pillar formation. More specifically, they examined several experimental parameters including relative humidity, temperature, pressure, droplet volume and initial contact angle, showing their influence on the final shape of the deposits; puddle or tall pillar. The effects of these parameters are combined into a dimensionless Péclet number $Pe = {h_0 j}/{D_c}$, which is the ratio of advection over

diffusive motion of the dissolved polymer, where j is the evaporative flux per unit area, h_0 is the initial height and D_C is the co-operative diffusion coefficient of the polymer.[28] The Péclet number is plotted against concentration in a phase diagram revealing that a clear boundary separates pillars and puddles with given initial parameters.[28] The experimental analysis showed that the final deposit of these heterogeneous elevated structures can sometimes be taller than the initial droplet height and all the dried polymeric material ends up nearly in the centre of the droplet, rather than distributed around the edge of the initial triple contact line i.e. the typical ring-stain effect.[28] Recently, Baldwin *et al.* [29] presented a semi-quantitative model comparing the opposing effects of advective build-up at the contact line to diffusive flux and used it to calculate a dimensionless number χ in order to predict which deposit will form. This ratio χ is similar to the Péclet number but it is constructed for the specific narrow wedge near the triple contact line, comparing the effective motions of flux and diffusion in this region: $\chi \approx \frac{K}{2\pi}\frac{c_0}{1-c_0}\frac{\dot{V}}{D_0 R \sin\theta}$, where K is a constant, D_0 is the self-diffusion coefficient, c_0 is the initial concentration, , θ is the contact angle and $\dot{V}$ is the overall evaporation rate. Analyzing the varying experimental parameters of concentration and flux, they showed that the boundary between flat puddles and pillars (monoliths) is at $\chi \approx 1.6$. They concluded that the drying behaviour of these droplets were defined by three critical factors; initial concentration, droplet geometry and evaporation rate.[29] In the latest work of Baldwin *et al.*[30], pillar (monolith) final formation was investigated with respect to: molecular weight, evaporation rate and polymer concentration of the PEO droplets. Various measurements demonstrated that the pillar (monolith) formation occurs over a limited range of molecular weights. They have also shown that values of Pe > 1 lead to a preferential deposition of the PEO solute at the contact line which can explain pillar formation for intermediate molecular weights.

However, the Péclet number argument does not account for the absence of pillars in high molecular weights.[30] They discussed the molecular weight dependence within various theoretical frameworks (e.g. viscoelasticity and diffusion) and they speculated upon the influence of contact line crystallization, viscosity, adhesion and friction phenomena. However, the variation of the end result (puddles or pillars) on molecular weight remains unexplained. It is important to determine how to control the evaporation mechanism and the final shape of the solute deposit for different molecular weights for both fundamental and application reasons. In this work, we use contact angle analysis to monitor the base radius, height, volume, surface area and contact angle of the droplet, at constant temperature, humidity and pressure, throughout the whole drying process for PEO with different molecular weights. This experimental technique provided valuable insights and revealed the differences in the underlying mechanisms that govern each stage of the drying process for each molecular weight used. Furthermore, we examined the drying process when the PEO solution droplets were placed upon glass slides covered by PEO films of different molecular weights. The results show clearly the importance of contact line and interface adhesion and friction effects. The evidently unique behaviour of droplets of PEO is a recent discovery; understanding all of the operating mechanisms that define the formation of the unusual-shaped deposits will be of a great practical importance.

Experimental method

Solutions were prepared using polymers (PEO) with various molecular weights: M_w = 10,000 g/mol (Sigma Aldrich 44101), 100,000 g/mol (Sigma Aldrich 181986), 200,000 g/mol (Sigma Aldrich 181994) and 300,000 g/mol (Sigma Aldrich 182001). All solutions

which were prepared with initial concentration c_0 = 10% by mass (which corresponds to close to the semidilute region for the lowest M_w and well into the semidilute region for the rest),[30] were mixed using distilled, de-ionised water and were left to equilibrate for at least 24 hours before use. A roller mixer was used to increase the dissolution rate. Mechanical mixing methods (vortex mixer, centrifuge or sonicator) were not used to prevent possible molecular damage. After mixing, cloudy undissolved polymer clusters appeared in our samples. These clusters were successfully removed from all samples by driving them through a 0.45 μm filter with an adjustable speed syringe pump at around 0.5 mL per hour. Filtering samples in order to remove undissolved clusters, resulted in slightly reducing the overall concentration (and also density ρ). A comparison of the concentrations of the solutions before and after filtering showed that there is a very small difference (<5%) for all molecular weights (see Fig. S1 supporting information). The method used for the removal of aggregates does not damage the polymer molecules.[28] For each measurement a droplet with an initial concentration of 10% and with a volume in the range from 1 μL to 5 μL was placed onto an ethanol-cleaned borosilicate glass microscope coverslip (dimensions: 24 mm × 50 mm × 100 μm from TAAB Laboratories Equipment Ltd, England). Furthermore, silicon wafers spin coated with an 1 μm thick poly(tetrafluoroethylene) (PTFE) layer were used in this work. The wafer was then cut into 1 × 1 cm^2 samples. PTFE substrates were cleaned before use in an ultrasonic bath of iso-propanol for at least 10 minutes. The droplets were deposited using a 1 mL syringe with a 0.71 mm diameter syringe needle. Despite the large shear rates in the needle (~100 s^{-1}), no significant differences in drying behaviour were seen when compared with droplets deposited less controllably by pouring, so we assume the polymer molecules are undamaged. A digital camera and a diffuse light source placed on either side of the droplet were used to record the whole evaporation process. Care was taken to place the

glass coverslip horizontally (a spirit level was used) and to reduce convective air currents around the droplet due to the light source. Digital images of the drying droplets were recorded at about 10 second intervals and analyzed using the dynamic contact angle analyser (FTÅ200, First Ten Ångstroms, Inc., Portsmouth) software. At early times of the evaporation process when the droplet was a spherical cap, the profile was fitted using the Young-Laplace equation[31] and values for the droplet base radius r, height h, volume V, surface area A and contact angle θ were extracted. However, once the deposition growth of the polymeric material began and the liquid droplet was resting on the solid deposit, the Young-Laplace equation could no longer be used to model the entire surface. Instead the two dimensional droplet profile was extracted from the recorded images using Image J 1.46m version (2011, US National Institutes of Health) and the surface area A and volume V of (the profile) rotation calculated numerically in PCO – Pictures (DocSchneider Engineering & Technical Software CH-8308 Illnau, Switzerland). Values of the deposit base radius r, height h, volume V are calculated by numerically integrating the digitised deposit profiles. The measurements were taken under controlled (relative humidity RH = 50 ± 5%, temperature T = 22 ± 1^{o}C, and pressure P = 1 atm) environmental conditions and droplet parameters, such as initial volume V_0, were systematically altered with a constant initial concentration of 10% by mass for all the droplets. After initial deposition of the droplet on the bare glass coverslip, the contact line became pinned at approximately between 60^{o} and 75^{o} with the vast majority between 65^{o} and 70^{o}. Additional experiments were carried out with glass substrates coated with PEO films prepared from 1 or 10% wt. PEO solutions with two different molecular weights: 10,000 or 100,000 g/mol. Spin coating was used to deposit thin and ultrathin PEO films on the flat glass substrates. A small amount of PEO solution was applied on the centre of the substrate span at 2,000 rpm at duratios of either 90 or 120 s. Moreover, dip coating

was used to prepare thicker absorbed PEO films. Topography images and/or height profiles of the PEO films were acquired by surface profilometry and atomic force microscopy (AFM). A Surface Roughness Tester, SURFTEST SJ-410 Series (Mitutoyo Corporation, Japan), was used for the height profiles of the thicker films. AFM imaging for the thin PEO films was conducted using a Bruker MultiMode Nanoscope IIIa AFM (Bruker AXS, Santa Barbara, CA), equipped with a J scanner (x–y scan range ~140 μm). The samples were imaged in tapping mode (tip in intermediate contact with the surface). Acquired images were post-processed by levelling and analysis (including height profiles) using the software Gwyddion,[32] a modular program for scanning probe microscopy (SPM) data visualization and analysis. The thickness was measured by taking profiles and/or images at the edge of the films and/or at areas where we scratched the polymer layer by a thin scriber (see supporting information for the height profiles and images). The films were continuous apart from the very thin ones (~20 nm thickness) where in some areas the film broke and the substrate was revealed (as shown in supporting information in Figure S2). In the case of the PEO solution droplet deposition on the PEO films, there was an initial spreading (for few tens or hundreds of seconds depending on the molecular weight) until pinning at about 25^o - 55^o degrees. The thickness range of the thinner films were found to be from ~20 nm to ~4 μm andwere associated with lower pinned contact angles at about 25^o - 35^o while thicker films: from ~30 to 280 μm gave pinned contact angles at about 35^o - 55^o.

Results

Figure 1 shows images of the drying process for 10% wt. PEO droplets with initial volumes of 3 μL, for the four different molecular weights, M_w. It is clear from the images that there are differences in drying behaviour for the different molecular weights. In

Figure 2 and 3, we present typical examples showing the whole evolution of the evaporation mechanism. Each graph shows the time sequence of contact angle and base radius profiles of 10% wt. PEO droplets of volumes, 1, 3 and 5 μL. Pinned contact line drying behaviour is shown during stage I; the droplet having a constant base radius r. Contact angle θ and height h both decrease in order to compensate for the reducing volume of the droplet. As the evaporation rate is greater at the triple contact line the liquid flows radially outwards in order to sustain the pinned droplet.[4] When the polymer concentration at the contact line becomes sufficiently high, precipitation of solid, semicrystalline spherulites of PEO will occur.[28] This should correspond to the (local) saturation c_{sat} (ca. $c_{sat} \approx 0.6$ by mass and approximately independent of M_w).[3] We hypothesize that the resulting deposit hinders radial, liquid flow by the creation of a "wall" of solid polymer separating evaporation flux and liquid replenishment. This effectively shifts the evaporation/flow continuity radially inwards. As this process continues during what we term stage II, the results will be a thin "carpet" of polymer left behind as the contact line recedes. As can be seen in Figures 2 and 3, the pinning stage takes considerably different times for the various molecular weights. The lowest duration of stage I is observed in the case of 100,000 g/mol, while in the case of 300,000 g/mol the droplet remained pinned for the whole evaporation process.

As suggested, during stage II the contact line recedes (base radius r decreases) and a thin layer of deposit is left behind. Contact angle and height h continue to decrease generally, but more slowly than in the previous stage. This effect may be expected on geometric grounds if the evaporation rate remains essentially unchanged. In the case of 10,000 g/mol in particular, the contact angle shows a plateau or a small increase for a short time after contact line depinning. Stage III (bootstrap growth) commences when the droplet (at

concentration c_{sat}) starts to be lifted upwards by the solid PEO precipitate. In this stage, apparent contact angle θ and height h increase. However, the base radius, r, decreases as the contact line recedes until the solvent is completely evaporated. During this stage, the droplet seems to push itself upwards.[26] This is clearest in the case of 100,000 g/mol where higher pillars are observed (and absent for 300,000 g/mol where no pillars are observed). This stage ends when the overall polymeric structure reaches its maximum height and all of the polymeric phase has precipitated as semi-crystalline spherulites. Water may still be trapped within the solid phase which leads to stage IV: the remaining liquid is encapsulated by solid PEO and the evaporation rate reduces considerably. However, because this specific phase can be very slow, we cannot measure its duration. The opacity of the final, dry, deposit gives an indication of its desiccation. It is worth noting that the forces generated during stage IV by the shrinking structure adhering to the coverslip can be strong enough to cause bending upwards of the latter.[33, 34, 35] Remarkably, droplets with the highest molecular weight PEO, M_w = 300,000 g/mol, never reach stage III (Figures 1 and 3); height h steadily decreases and the final deposit is a flat "puddle", with a quite constant thickness. Interestingly, for these droplets there is some evidence for a slight reduction or fall in base radius r (and simultaneously small increase of contact angle θ) but this is not sustained and the system remains pinned followed by late drying occurring to some extent simultaneously.

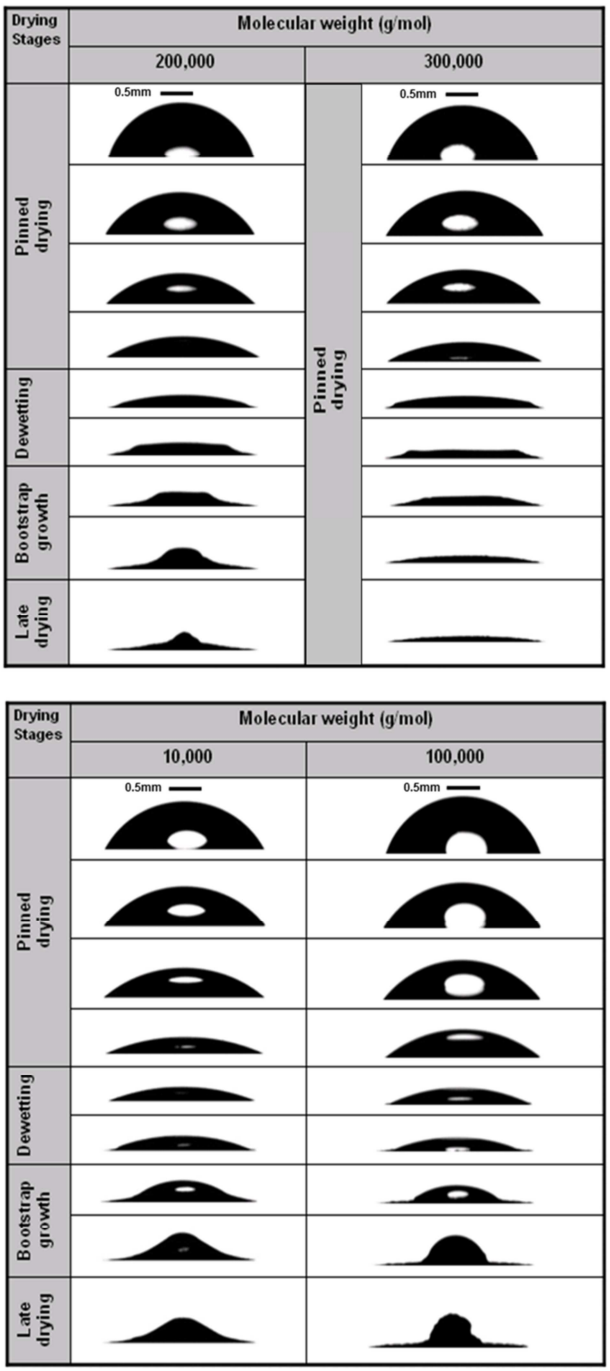

Figure 1. Example of the evaporation process for 10% wt PEO droplets with volume 3 μL for the four different molecular weights M_w via the characteristic four stage drying mechanism: Stage I, pinned drying; stage II, dewetting; stage III, bootstrap growth and stage IV, late drying, at ambient conditions. The scale bar represents 0.5 mm.

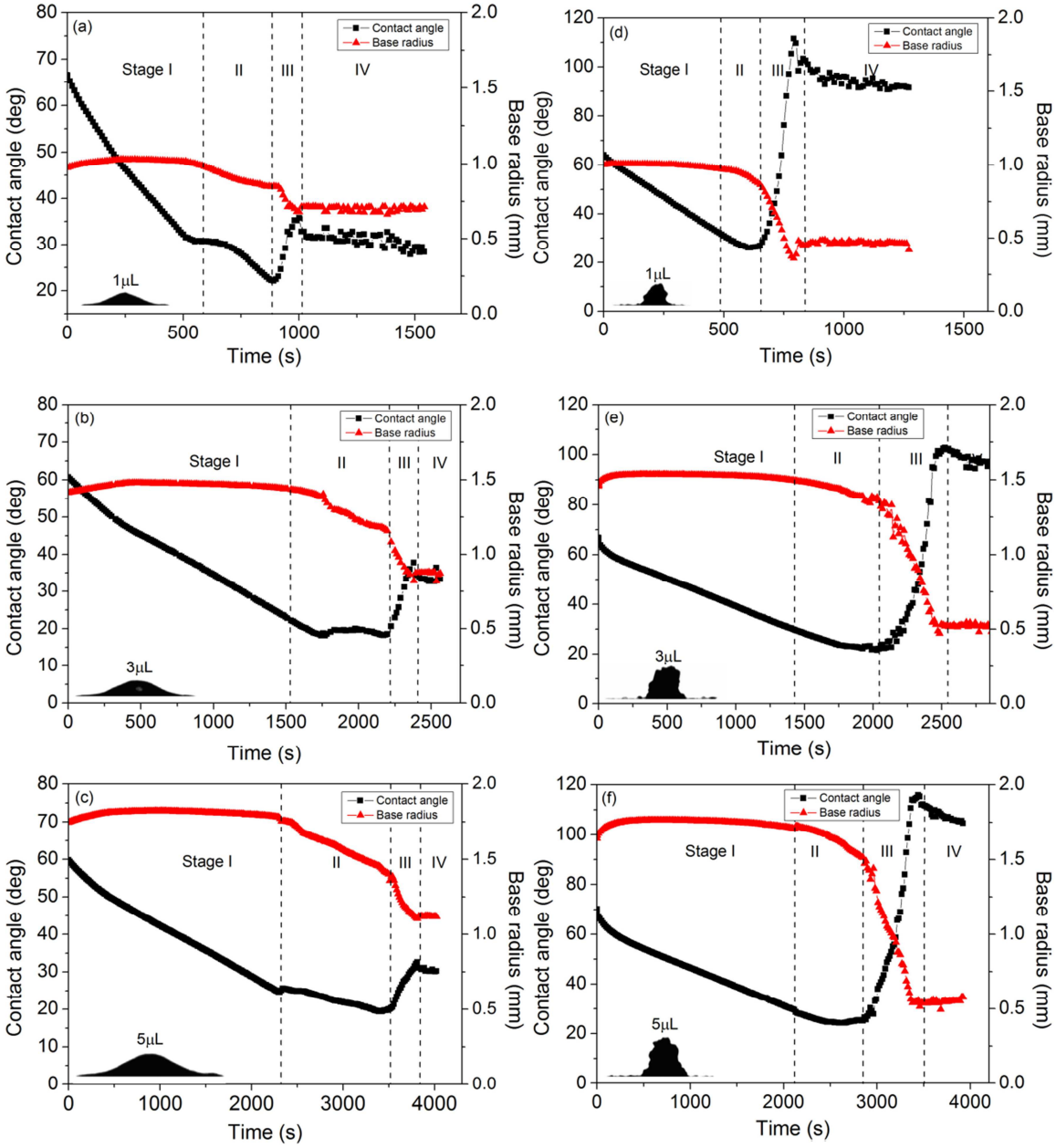

Figure 2. Contact angle, θ (degrees) and base radius profiles, r (mm) analysis in time (s) for (a: 1, b: 3, c: 5 μL) 10,000 g/mol and (d: 1, e: 3, f: 5 μL) 100,000 g/mol during the evolution of the whole evaporation process (representative examples from ~25 repetitions for each M_w). Black squares correspond to contact angle measurements and red triangles depict base radius measurements. Uncertainties, at later times t, in base radius and contact angle θ are due to deviations of the shape of the droplet as material is deposited. Insets depict the final PEO deposits.

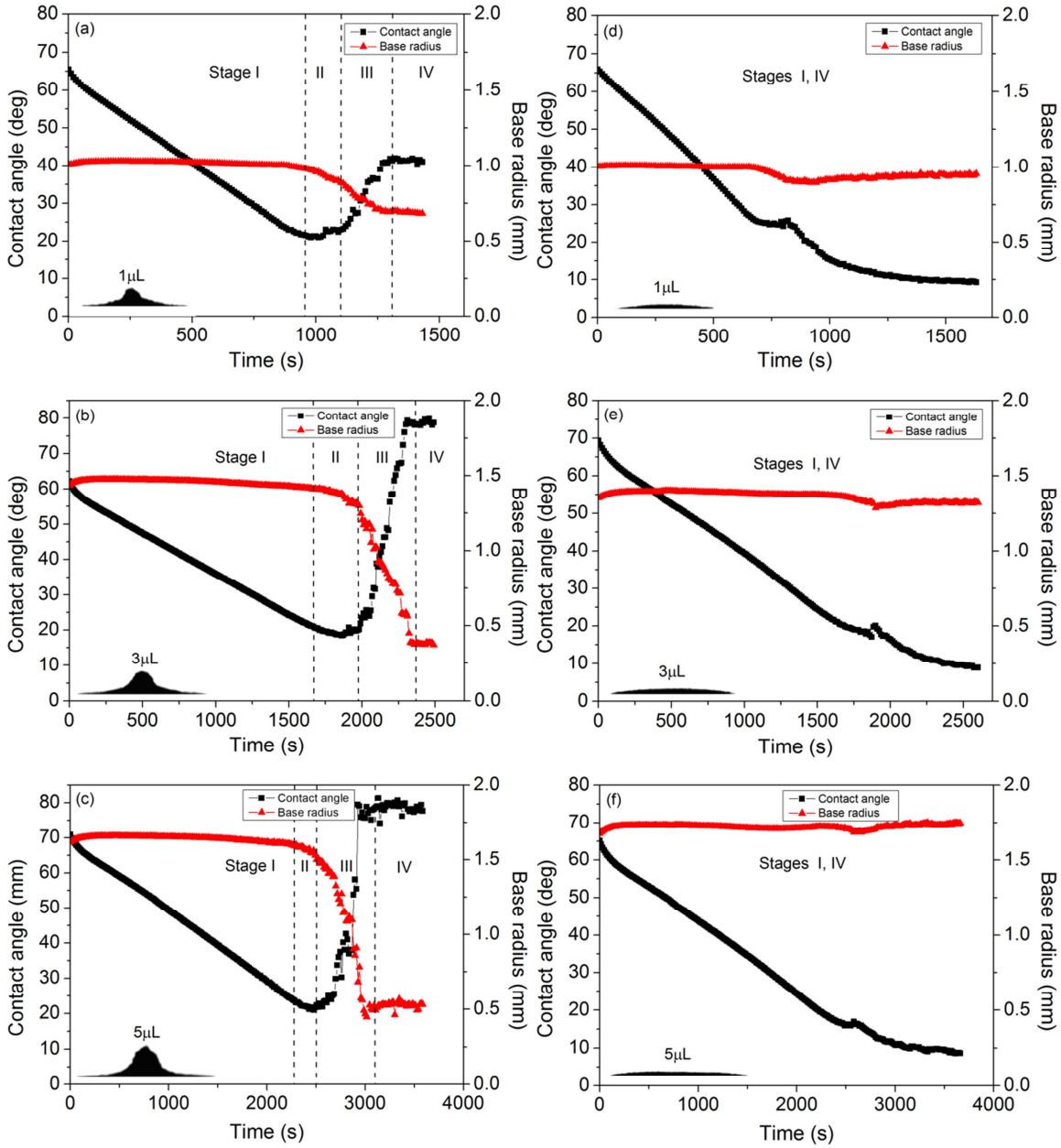

Figure 3. Contact angle, θ (degrees) and base radius profiles, r (mm) analysis in time (s) for (a: 1, b: 3, c: 5 μL) 200,000 g/mol and and (d: 1, e: 3, f: 5 μL) 300,000 g/mol during the evolution of the whole evaporation process (representative examples from ~25 repetitions for each M_w). Black squares correspond to contact angle measurements and red triangles depict base radius measurements. Uncertainties, at later times t, in base radius and contact angle θ are due to deviations of the shape of the droplet as material is deposited. Insets depict the final PEO deposits (pillars or puddles).

The average duration of the pinning stages during the drying process are presented in Figure 4a. These are plotted against the four different values of M_w for drop volumes from 1 μL to 5 μL (~25 individual experiments for each M_w). The time period of pinning (stick time) for M_w = 10,000 g/mol is longer than for M_w = 100,000 g/mol, suggesting that a different mechanism is taking place in the vicinity of the contact line. The pinning period increases from M_w = 100,000 g/mol to M_w = 200,000 g/mol (Figure 4) and results in different final pillar formation morphology. It is worthwhile noting that the 200,000 g/mol case behaves similarly to the 10,000 g/mol case: almost the same pinning time periods leading to relatively low pillars of similar shape. In contrast to all the previous observations, for droplets with M_w = 300,000 g/mol there was continuous pinning and no pillar formation can be seen in Figure 3(d, e, f). For the case of 300,000 g/mol, the droplet is pinned throughout the evarporation process and thus the corresponding times in Fig. 4a are total evaporation times. In Fig 4b, we plotted the variation of normalised pinning time (=pinning time/total evaporation time) for the four different molecular weights. The pinning time values for the different volumes cluster (especially for the higher moleculare weights) and show more clearly the non-linear dependence against the M_w and the local minimum at 100,000 g/mol for all volumes. The depinning mechanism seems to be an essential phase to pillar (monolith) formation, as the solid polymeric material must follow the trace of the droplet inward to the centre. On the contrary, if the droplet contact line remains stationary, then pillar formation is suppressed and a puddle appears. As the pinning stage (stick time) increased, it discouraged pillar formation. The possible origins of these phenomena at the triple phase contact line are discussed later.

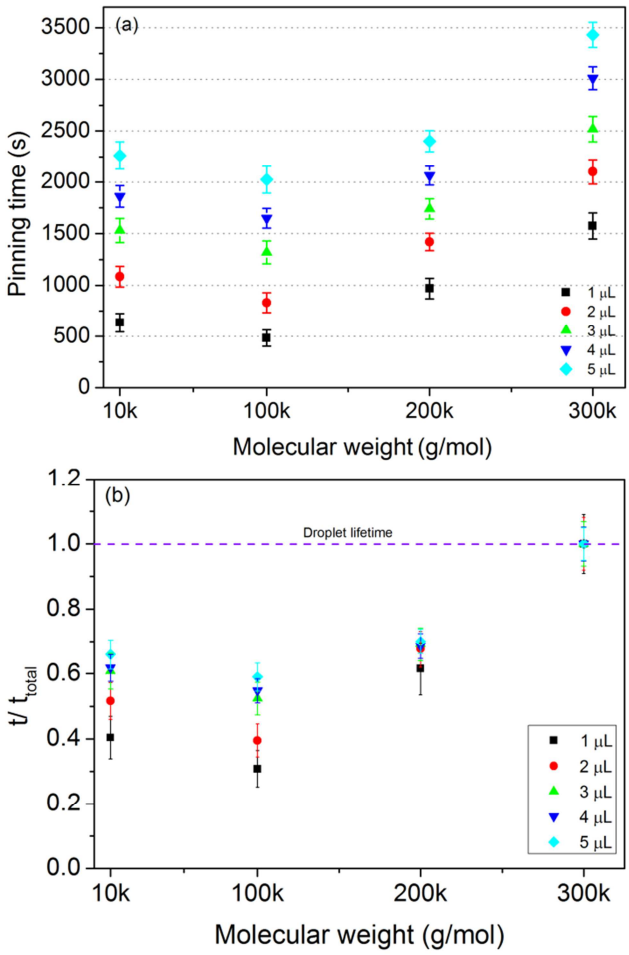

Figure 4. (a) Average times of the pinning stage over the four different molecular weights for the 10% wt PEO droplets in a range of initial volumes (1 µL – 5 µL) and (b) the normalised pinning time values for the four different molecular weights.

Figure 5 shows typical images of the final PEO deposits for the different M_w and volumes used (5 or 6 repetitions for each case). The final dried polymeric material exhibits a variety of shapes and final volumes depending on the M_w and droplet volume (1 µL to 5 µL), respectively. For PEO droplets with M_w = 10,000 g/mol, the final morphology of the dried solutes was a low smooth conical pillar (monolith). Droplets with M_w = 100,000 g/mol displayed final deposits formed as solid tall, steep and rough pillars (monoliths), several millimetres in height, sometimes over twice the initial height h_0, usually at or near the centre of the substrate. The profile of these droplets exhibited characteristic steep

rough surfaces. For M_w = 200,000 g/mol, final solid precipitates were again tall and in the form of rough pillars (monoliths), reaching a maximum height h_{max}, lower than the previous case (M_w = 100,000 g/mol), where the edge extended almost to the initial base radius r_0. Finally, for M_w = 300,000 g/mol, smooth disk-like puddle formations can be seen (Figure 5) with a final base radius equal to the initial droplet base radius r_0.

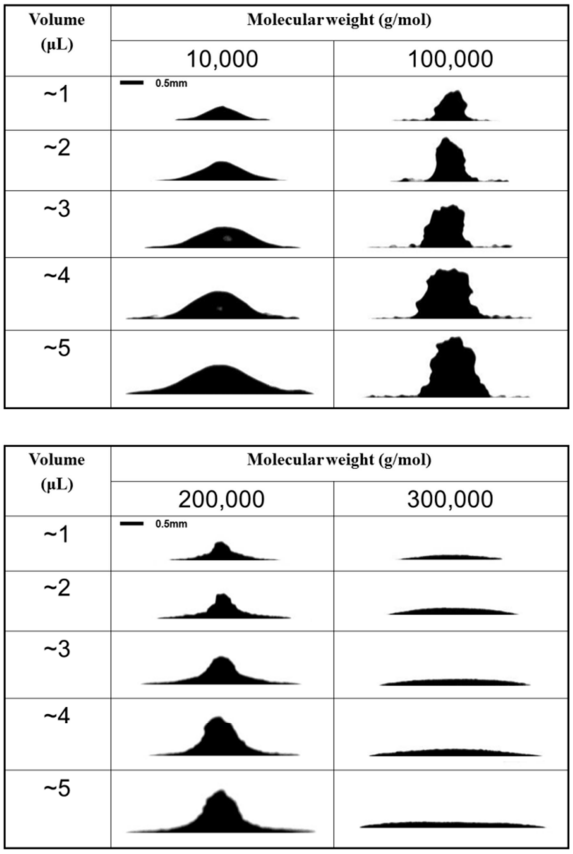

Figure 5. Samples of final deposits (pillars or puddles) from 1 μL to 5 μL droplets containing 10% wt. PEO with M_w = 10, 100, 200 and 300 kg/mol; representative examples from ~5-6 repetitions for each case (molecular weight and volume),. Note the preferential formation of high pillars at M_w = 100,000 g/mol and the formation of a flat puddle for droplets with M_w = 300,000 g/mol. The scale bar is 0.5 mm.

Figure 6(a - d) depicts the graphs of the aspect ratio (final height over the base diameter) of either pillar or puddle formation of the final PEO deposits versus the initial volumes of the PEO droplets for the four M_w. Altering the initial volume of the droplet does not drastically influence the behaviour of the dried PEO solute at the end of the evaporation process over a range from 1 µL to 5 µL. Figure 6e presents the average aspect ratio for each of the four molecular weights. It is clearly illustrated in Figure 6e that for higher final pillar formation, droplets with M_w = 100,000 g/mol, we obtain a much higher average aspect ratio and the reverse result is shown for droplets with high molecular weight (M_w = 300,000 g/mol), where the final shape is only flat disks.

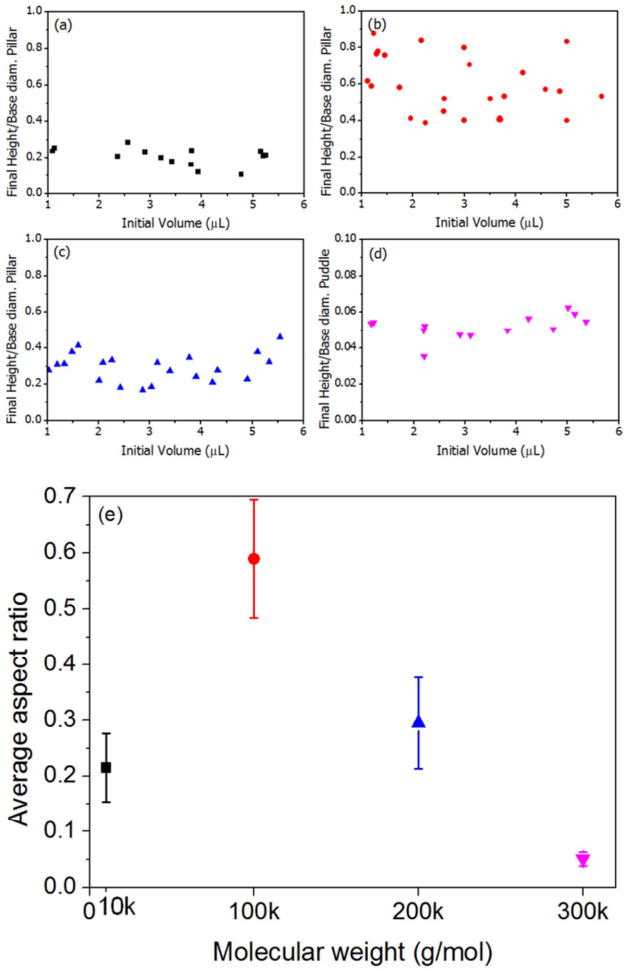

Figure 6. Aspect ratio (final height of pillar or puddle formation (mm) / base diameter of pillar or puddle (mm) formation) of PEO solutions samples plotted for the four different molecular

weights (a: 10 k, b: 100 k, c: 200 k and d: 300 kg/mol). Note that aspect ratio measurements for M_w = 300 kg/mol are plotted on a different scale due to the very low disk-like shape of the final PEO deposits. (e) Average aspect ratio measurements of PEO solutions samples for each M_w.

Additionally, we estimated the *void fraction* (fraction of the volume of voids in a material over the solid volume of the material), of the final PEO deposits. In other words, we calculated the difference between the measured final volume of the deposit and the volume of the solid deposit based on the concentration 10% wt. of PEO in every droplet and the volume of the droplet, divided by the solid volume of the deposits ($\frac{V_m}{V_s} - 1$); where V_m is the measured final volume of the deposits and V_s is the calculated solid volume. Figure 7 depicts the void fraction results as a function of the initial volume of the droplets. Void fraction measurements (Figure 7) show that only in the case of droplets with M_w = 100,000 g /mol did we obtain values significantly deviating from zero (higher void fraction), in contrast to the other molecular weights that are quite close to the zero line with low void fraction. The presence of voids inside the solid final deposits, for droplets with M_w = 100,000 g /mol with higher pillar formation, could be explained by the frequent appearance of a hollow region (at the pillar base, near the substrate) as viewed from underneath the final deposits. This observation is consistent with the experimental results presented in the previous work by Willmer *et al.*[26] and could indicate low interfacial adhesion between the droplet and the substrate for the M_w that produces high pillars.

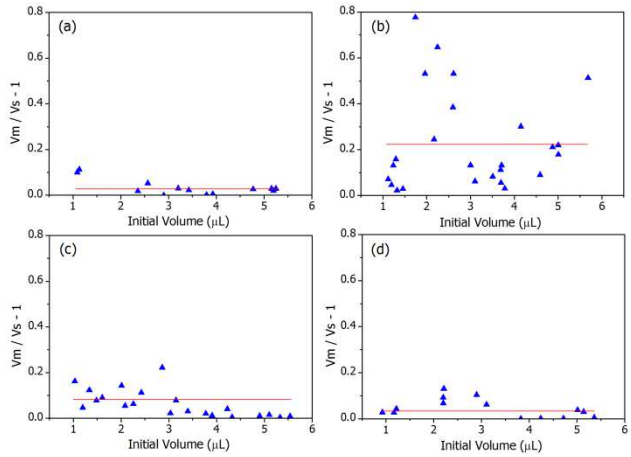

Figure 7. Void fraction calculations for the four different molecular weights (a: 10 k, b: 100 k, c: 200 k and d: 300 kg/mol) of the 10% wt PEO droplets plotted as a function of the initial droplet volume (μL). Note that the values which are closer to zero line indicate fewer voids compared with the other cases. The horizontal red line signifies the average value for each molecular weight.

Additional experiments were carried out to investigate the effect of interfacial interactions at the contact line for the specific case of the highest molecular weight which produces puddle shaped deposits. Figure 8 shows typical examples (~ 4-5 μL volumes, >5 experiments for each thickness) of the 300,000 g /mol 10% PEO droplets evaporation process on substrates covered with a PEO film (casted by 10% by mass PEO solutions and dried out on glass coverslips, ~ 200 μm thickness) of 10,000 g /mol and 100,000 g /mol molecular weights, respectively. In both cases, the 300,000 g /mol 10% PEO droplet dried out resulting in pillar formation morphology (aspect ratios 0.2-0.4). In Figure 9, contact angle θ and base radius r profiles show the drying process. The PEO droplet spreads when it contacts the PEO film and following this, there is a period with approximately pinned contact line. This initial spreading is more pronounced for the 100,000 g/mol films. Stages II (depinning) & III (bootstrap growth) take place at the same time with a receding contact line and an increasing contact angle θ (and height h). It is

well known that pillar formation is inhibited by low contact angles (even for the favourable for pillar formation 100,000 g/mol PEO).[28] The pinned contact angles were higher (35^o - 55^o) for thicker films (~30-280 μm). Additional experiments have been done with lower thickness of the 10,000 and 100,000 g/mol PEO films from ~20 nm to ~4 μm and in all cases, samples either ended up in a disk-like formation or the resulting peaks were of much lower aspect ratio. It should be noted though, that for such thinner films, the droplets spread more and become pinned at much smaller contact angles (25^o - 35^o) compared to both the droplets placed directly on glass slides (60^o - 75^o) and to thicker dip-coated PEO films (35^o - 55^o). Thus, the absence of pillars in these cases can be associated with these low contact angles.

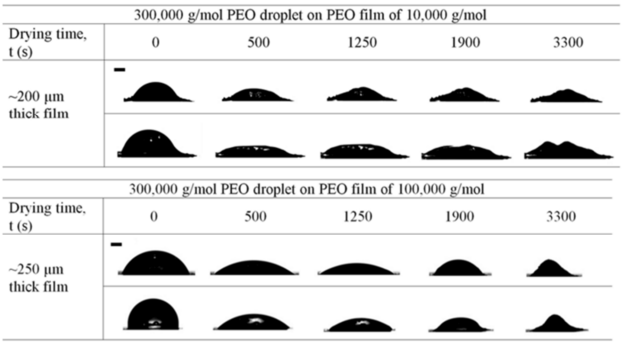

Figure 8. Examples of time lapse profile images of 300,000 g /mol PEO droplets (~ 4-5 μL volumes) with initial concentration c_0 = 0.1 by mass placed on PEO films of 10,000 g /mol (above) and 100,000 g /mol (below), during the whole drying process in ambient conditions. The scale bar represents a width of 0.5 mm (times are approximate).

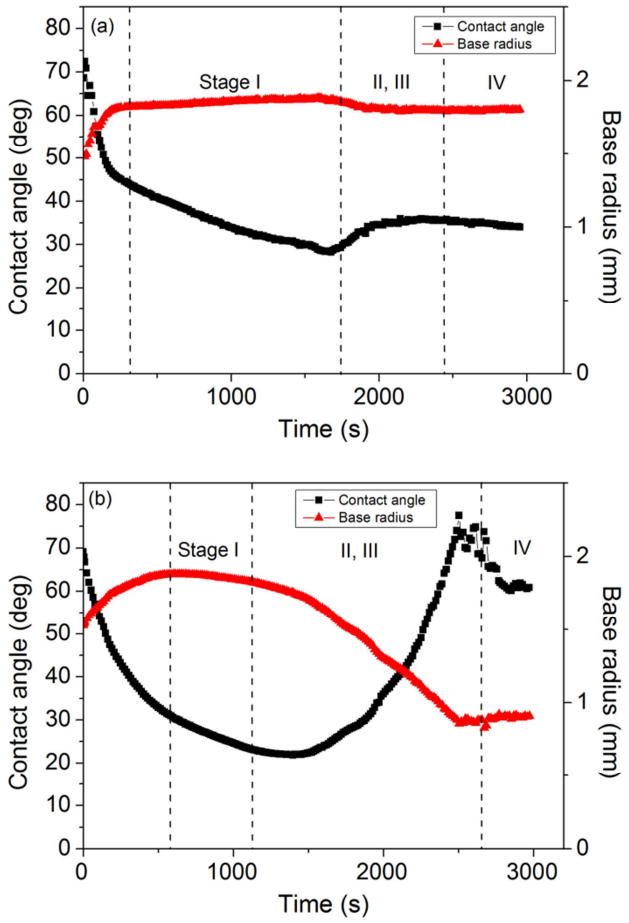

Figure 9. Contact angle, θ (degrees), and base radius profiles, r (mm), vs time (s) for 300,000 g/mol PEO droplets placed (~4-5 μL volume) on (a) 10,000 g/mol and (b) 100,000 g/mol PEO films during the evolution of the whole evaporation process (representative examples from ~5 repetitions for each M_w). Black squares correspond to contact angle measurements and red triangles depict base radius measurements. Uncertainties, at later times t, in base radius and contact angle θ are due to deviations of the shape of the droplet as material is deposited.

Another set of experiments was carried out to further investigate the role of adhesive and friction interactions of the PEO droplets with high molecular weight at the proximity region of the contact line. We used poly(tetrafluoroethylene) (PTFE) substrates to minimize the work of adhesion and friction phenomena.[36, 37] In Fig 10, we present a typical example of a 10% wt. PEO droplet with M_w = 300k g/mol (we performed 15 repetitions for this substrate) showing the whole evaporation process. The graph shows

the time sequence of contact angle and base radius profiles of a 3 μL droplet. In the beginning, the PEO droplet follows a pinned contact line behaviour (Stage I) for a small time period. Depinning occurs as it can be clearly seen by the decrease of the contact radius which signifies that start of Stage II (dewetting). Stage III (bootstrap growth) follows with the characteristic increasing of the contact angle θ (and height h). At last, the late drying stage occurs resulting in a pillar structure formation. It is worth noting that the vast majority of the PEO material is dragged towards the centre of the liquid droplet (Fig 10 top view image) leaving behind a thin trace of PEO.

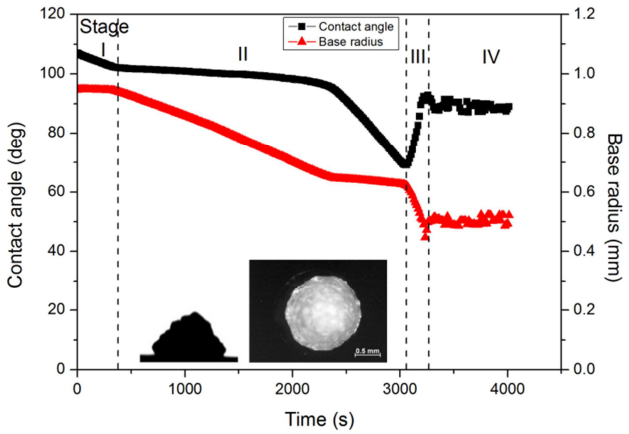

Fig 10. Contact angle, θ (degrees) and base radius profiles, r (mm) versus time (s) for a 3 μL PEO 10% wt. solution droplet of 300k g/mol molecular weight on a PTFE substrate during the whole evaporation process under ambient conditions. Black squares correspond to contact angle and red triangles to base radius measurements. Uncertainties, at later times t, in contact angle and base radius are due to deviations of the shape of the droplet as PEO material is deposited. Inset depicts the final PEO deposit extracted from FTA software (side view) and from stereo microscope (top view).

Discussion

It is well known that the evaporation of droplets on hydrophilic substrates occurs mainly at the triple contact line (TCL).[4] During stage I of the evaporation process the local, higher evaporation flux near the pinned contact line, *j*, induces an outward, radial flow to replace the reducing volume of the remaining liquid. This increases the PEO concentration (ultimately) to c_{sat} locally (at TCL). Once the first spherulites have been deposited, the evaporation at the contact line is disturbed, as discussed above, which in turn impedes radial flow and thus depinning occurs. However, diffusion opposes this motion and tends to drive the polymer solution to homogeneity.[28] For this reason, the outward liquid flow, induced by the effect of evaporative flux at the contact line, must be greater than the effect of polymer diffusion in order to have a build-up of polymeric material at the TCL. Previous studies from Baldwin *et al.* [28] showed that the Péclet number ($Pe = h_0\, j / D_G$) can be used to explain the competition between these opposing trends. A low Péclet number would lead to small concentration gradients, without preferential deposition at the edge and result in a puddle-like final deposit.[28] In contrast, a high Péclet number would result in early crystallization of the polymer at the contact line and a final pillar-shape deposit to occur.[28] The time until c_{sat} is reached at the TCL, and the liquid droplet depins, depends on how quickly polymer chains can move away from the contact line, and hence depends on the M_w. The value of the gradient diffusion coefficient includes a concentration dependent term[38] which is correlated to M_w: $D_G \sim D_0 (c^*/c)^{1/2} \sim M_w^{-1}$ (for semidilute entangled solutions), where c^* ($\sim M_w / R_g^3 \sim M_w^{-4/5}$) is the overlap concentration of the solution, R_g is the radius of gyration and D_0 is the self-diffucion coefficient. Thus, for droplets with low molecular weight (M_w = 10,000 g/mol), polymer chains diffused away from the TCL region more quickly and were unable to reach sufficiently quickly the precipitation concentration. They remained pinned for

longer times than those with 100,000 g/mol molecular weight (Figure 4), thus preventing high pillar formation. In higher molecular weight polymers (M_w = 100,000 g/mol), on the other hand, a drastic decrease of the diffusion leads to an earlier accumulation of the polymer chains at the contact line resulting in early depinning and hence high pillar formation. By extrapolation, one would expect that PEO droplets with M_w = 200,000 and 300,000 g/mol would result in easier accumulation at the contact line due to the further decrease in chain diffusion, leading to even earlier crystallization and depinning and in turn higher pillar morphology. However, this was not seen; on the contrary an increase in the pinning times is observed for these droplets leading to lower pillars for 200,000 g/mol and very flat puddles for 300,000 g/mol. Therefore, another mechanism must have become dominant in these cases. It is clear from our experimental results that the critical experimental parameter that determines the final morphology is the time period until deposition starts at the TCL (i.e. pinning stage).

The experiments involving the deposition of the 300,000 g/mol droplets on 10,000 or 100,000 g/mol and PTFE films show significant differences compared to results obtained on glass and indicate that phenomena taking place at the interface are of importance. The force balance for fluid – solid systems under dynamic conditions consists of capillary forces which are opposed by the friction of the substrate as the fluid advances or recedes. For the general case of a solid–liquid–vapor system, the contact line friction was found to increase linearly with liquid viscosity and exponentially with the work of adhesion.[39] The polymer chain length is a parameter which could drastically modify the adherence energy of the fluid with the substrate and the interfacial dissipation phenomena at the contact line. Polymer chains are attracted by the substrate (van der Waals, hydrogen bonds etc.) and tend to increase the number of monomers in contact with the surface in order to gain

adsorption energy, but they are confined and thus lose (conformational) entropy.[38, 40] Therefore, large polymer chains adsorb more strongly on solids;[41, 42] as experimentally verified for the PEO/glass system in particular.[43, 44, 45, 46] When polymers contact a solid surface, an adsorbed layer is formed fairly quickly, even if the bulk solution is dilute.[41] The adsorbed polymer layer thickness depends on the molecular weight and is characterised by a small number of *long* 'loops' and 'tails' [47, 48] that can extend into the solution and modify the interfacial energy of the system.[45, 49, 50] The loops and tails are more prominent and longer for larger molecular weights. The energy of adhesion and frictional stress of a polymer network with an adsorbed polymer layer were found to increase both with the M_w of the adsorbed layer and the M_w of the chains between the (physical or chemical) crosslinks (with the exception of high grafting densities).[51, 52, 53, 54, 55] The loops and tail ends of the absorbed high M_w chains intertwine with the inter-connected polymer network increasing the (interfacial) adhesion energy of the system.[42, 49, 50, 54] Thus, a significant part of the energy of the system is dissipated within this region as a result of cohesive interactions and entanglements for sufficiently high molecular weights.[54] In our system, for high M_w PEO, a polymer film with long loops and tails forms on the substrate which interlace into the dense polymer network formed within the droplet as the water evaporates. This adhesive effect *inhibits* the polymer chain network (gel in our case) from moving and thus depinning cannot readily occur because the dense polymer solution droplet is fixed by the loops and tails of the strongly adsorbed layer. PEO can adsorb fairly strongly on the glass by hydrogen bonding as already measured.[43, 44, 45] These ideas provide us with an insight about the possible friction phenomena generated at the contact line in our system. These can explain the behaviour of droplets with M_w = 200,000 and 300,000 g/mol on glass, where the work of adhesion and the contact line friction become dominant in the system and control the drying mechanism.

The energy dissipation of the system through enhancement of the frictional resistance at the contact line and the work of adhesion of high M_w polymer chains led the system to follow typical pinned behaviour for long times and in particular for the highest M_w of this study during the whole evaporation process. In contrast, for droplets with M_w = 10,000 and 100,000 g/mol these interface phenomena are not prominent enough to influence drastically the pinning stage and the depinning transition due to the relatively small molecular weight (Figs 3 & 4). Presumably, for the droplets on glass, the minimum of pinning time exists around M_w = 100,000 g/mol where the two effects (bulk diffusion and interface adhesion) discussed are becoming less prominent and pillar formation can occur.

Contrary to the situation on glass, in the experiments involving the deposition of the 300,000 g/mol droplets on 10,000 or 100,000 g/mol films, the already preformed film of lower molecular weight PEO prevents the adsorption of the long 300,000 g/mol chains and thus interfacial interactions and friction are much weaker. This is further verified by the case of the deposition of the 300,000 g/mol droplets on PTFE films where the interfacial interactions and friction are lower (owing to the chemical nature of the PTFE) and we observe clearly depinning and pillar formation.

An interesting point that deserves some attention is the issue of precipitation-induced depinning as described in previous work.[26, 28, 29, 30] in combination with evidence that the precipitation of the higher molecular weight droplet starts first (Figure 4 in Ref. [30]). This is not unexpected as there is less diffusion and c_{sat} (~0.6 for all mol. weights) can be reached more rapidly. However, there is no doubt after our study that for higher molecular weights (particularly 300k) that the depinning and dewetting (on glass) does

not happen. In view of our results and analysis, we can now conclude that the precipitation is not a sufficient condition for depinning and dewetting. In addition, the polymer droplet needs to have the necessary “freedom” to move/slide laterally towards the centre. The interdigitation-induced adhesion with the adsorbed polymer layer inhibits the depinning although precipitation occurs earlier. At lower PEO molecular weight droplets (on glass) this interface effect is absent (chains are short and the adsorbed layer do not interdigitate so much with the polymer gel above) and precipitation (although coming later) induces depinning and dewetting.

Conclusions

We have studied the drying process of a semidilute PEO droplet deposited on a planar solid surface (glass coverslip), planar PEO (formed on the glass coverslip) and PTFE films (formed on a silicon wafer). The shape of the final solid deposits on glass was found to depend strongly on the molecular weight with high pillars favoured for intermediate molecular weights (100,000 g/mol and 200,000 g/mol) while higher molecular weights (300,000 g/mol) formed flat puddles. We have identified that the duration of the pinning stage is crucial for the final morphology of the polymeric deposits. Long pinning times are associated with puddles or low aspect ratio pillars. The competition of the phenomena acting at the contact line and in the bulk of the fluid determine the length of the pinning stage until deposition of the first spherulites. Diffusion based arguments (Péclet number) can account for the absence of high pillars for low molecular weights but cannot explain puddle formation for high molecular weights. Our experiments involving high M_w PEO droplet evaporation on lower M_w PEO and PTFE films showed pillar formation and demonstrated that interface (polymer/substrate) phenomena can play a major role. For high M_w, intertwining between the long loops and tails of an adsorbed polymer layer and

the polymer gel network in the droplet can induce strong adhesion which retains the droplet in the pinning stage for the entire drying period. This interfacial phenomenon can explain the formation of puddles for the case of high M_w droplets on glass and may be an important contribution to the physics of the overall behavior in addition to the Péclet number arguments discussed in previous studies. It seems particularly crucial in order to interpret the results for the high M_w PEO droplets.

ASSOCIATED CONTENT

Supporting information

Further experimental details and characterization of the PEO films used in this work. This material is available free of charge via the Internet at http:// pubs.acs.org.

ACKNOWLEDGMENTS

This work was carried out under the umbrella of COST Action MP1106: “Smart and green interfaces—from single bubbles and drops to industrial, environmental and biomedical applications”. We acknowledge funding from the Engineering and Physical Sciences Council (EPSRC) DTA.

References

1. de Gans, B. J.; Duineveld, P. C.; Schubert, U. S. Inkjet printing of polymers: State of the art and future developments. *Adv Mater* **2004,** *16* (3), 203-213.
2. Lee, H. H.; Chou, K. S.; Huang, K. C. Inkjet printing of nanosized silver colloids. *Nanotechnology* **2005,** *16* (10), 2436-2441.
3. Sefiane, K.; Bennacher, R. An expression for droplet evaporation incorporating thermal effects. *Journal of Fluid Mechanics* **2011,** *667*, 260-271.
4. Deegan, R. D.; Bakajin, O.; Dupont, T. F.; Huber, G.; Nagel, S. R.; Witten, T. A. Capillary flow as the cause of ring stains from dried liquid drops. *Nature* **1997,** *389* (6653), 827-829.

5. Shen, X. Y.; Ho, C. M.; Wong, T. S. Minimal Size of Coffee Ring Structure *J Phys Chem B* **2010,** *114* (26), 8826-8826.
6. Hu, H.; Larson, R. G. Analysis of the Effects of Marangoni Stresses on the Microflow in an Evaporating Sessile Droplet. *Langmuir* **2005,** *21* (9), 3972-3980.
7. Marín, Á. G.; Gelderblom, H.; Lohse, D.; Snoeijer, J. H. Order-to-Disorder Transition in Ring-Shaped Colloidal Stains. *Phys Rev Lett* **2011,** *107* (8), 085502.
8. Yunker, P. J.; Still, T.; Lohr, M. A.; Yodh, A. G. Suppression of the coffee-ring effect by shape-dependent capillary interactions. *Nature* **2011,** *476* (7360), 308-311.
9. Rowan, S. M.; Newton, M. I.; Driewer, F. W.; McHale, G. Evaporation of microdroplets of azeotropic liquids. *J Phys Chem B* **2000,** *104* (34), 8217-8220.
10. Li, G. F.; Graf, K. Microstructures formation by deposition of toluene drops on polystyrene surface. *Phys Chem Chem Phys* **2009,** *11* (33), 7137-7144.
11. Parisse, F.; Allain, C. Drying of colloidal suspension droplets: Experimental study and profile renormalization. *Langmuir* **1997,** *13* (14), 3598-3602.
12. Pauchard, L.; Allain, C. Buckling instability induced by polymer solution drying. *Europhys Lett* **2003,** *62* (6), 897-903.
13. Stannard, A. Dewetting-mediated pattern formation in nanoparticle assemblies. *Journal of Physics: Condensed Matter* **2011,** *23* (8), 083001.
14. Hu, H.; Larson, R. G. Marangoni effect reverses coffee-ring depositions. *J Phys Chem B* **2006,** *110* (14), 7090-7094.
15. Pauchard, L.; Allain, C. Stable and unstable surface evolution during the drying of a polymer solution drop. *Phys Rev E* **2003,** *68* (5), 052801.
16. Fischer, B. J. Particle Convection in an Evaporating Colloidal Droplet. *Langmuir* **2001,** *18* (1), 60-67.
17. Freed-Brown, J. Evaporative deposition in receding drops. *Soft Matter* **2014,** *10* (47), 9506-9510.
18. Cox, L. R.; Dunlop, E. H.; North, A. M. Role of molecular aggregates in liquid drag reduction by polymers. *Nature* **1974,** *249* (5454), 243-245.
19. Israelachvili, J. The different faces of poly(ethylene glycol). *Proceedings of the National Academy of Sciences* **1997,** *94* (16), 8378-8379.
20. Hammouda, B. Solvation characteristics of a model water-soluble polymer. *Journal of Polymer Science Part B: Polymer Physics* **2006,** *44* (22), 3195-3199.
21. Hammouda, B.; Ho, D. L.; Kline, S. Insight into clustering in poly(ethylene oxide) solutions. *Macromolecules* **2004,** *37* (18), 6932-6937.
22. Wallstrom, L.; Lindberg, K. A. H. Wood Surface Stabilization with Polyethyleneglycol, Peg. *Wood Sci Technol* **1995,** *29* (2), 109-119.
23. Collyer, A. A. Turbulence and drag reduction: a macroscopic view (education). *Physics Education* **1975,** *10* (4), 305-311.
24. André, C. D.; Rachael, A. L.; Abraham, M. L.; Eric, W. K. Effects of Ammonium Sulfate and Sodium Chloride Concentration on PEG/Protein Liquid−Liquid Phase Separation. *Langmuir* **2008,** *24* (18), 10345-10351.
25. Abuchowski, A.; McCoy, J. R.; Palczuk, N. C.; van Es, T.; Davis, F. F. Effect of covalent attachment of polyethylene glycol on immunogenicity and circulating life of bovine liver catalase. *The Journal Of Biological Chemistry* **1977,** *252* (11), 3582-3586.
26. Willmer, D.; Baldwin, K. A.; Kwartnik, C.; Fairhurst, D. J. Growth of solid conical structures during multistage drying of sessile poly(ethylene oxide) droplets. *Phys Chem Chem Phys* **2010,** *12* (16), 3998-4004.
27. Willmer, D. Non-Equilibrium Polymeric Fluids. PhD, Nottingham Trent University2011.

28. Baldwin, K. A.; Granjard, M.; Willmer, D. I.; Sefiane, K.; Fairhurst, D. J. Drying and deposition of poly(ethylene oxide) droplets determined by Peclet number. *Soft Matter* **2011,** *7* (17), 7819-7826.
29. Baldwin, K. A.; Roest, S.; Fairhurst, D. J.; Sefiane, K.; Shanahan, M. E. R. Monolith formation and ring-stain suppression in low-pressure evaporation of poly(ethylene oxide) droplets. *Journal of Fluid Mechanics* **2012,** *695*, 321-329.
30. Baldwin, K. A.; Fairhurst, D. The effects of molecular weight, evaporation rate and polymer concentration on pillar formation in drying poly(ethylene oxide) droplets. *Colloid Surf. A-Physicochem. Eng. Asp.* **2014,** *441*, 867-871.
31. Rotenberg, Y.; Boruvka, L.; Neumann, A. W. Determination of Surface-Tension and Contact-Angle from the Shapes of Axisymmetric Fluid Interfaces. *J Colloid Interf Sci* **1983,** *93* (1), 169-183.
32. Nečas, D.; Klapetek, P. Gwyddion: an open-source software for SPM data analysis. *centr.eur.j.phys.* **2012,** *10* (1), 181-188.
33. Shanahan, M. E. R. Contact-angle equilibrium on thin elastic solids. *Journal of Adhesion* **1985,** *18* (4), 247-267.
34. Shanahan, M. E. R. Equilibrium of liquid-drops on thin plates - plate rigidity and stability considerations. *Journal of Adhesion* **1987,** *20* (4), 261-274.
35. Francis, L. F.; McCormick, A. V.; Vaessen, D. M.; Payne, J. A. Development and measurement of stress in polymer coatings. *J Mater Sci* **2002,** *37* (22), 4717-4731.
36. Cheng, X.; Xue, Y.; Xie, C. Tribological investigation of PTFE composite filled with lead and rare earths-modified glass fiber. *Materials Letters* **2003,** *57* (16–17), 2553-2557.
37. Ebnesajjad, S. Discovery and History of Fluoropolymers. In *Introduction to Fluoropolymers*; William Andrew Publishing: Oxford, 2013; Vol. 3, pp 17-35.
38. Rubinstein, M.; Colby, R. H. *Polymer Physics*; Oxford University Press: Oxford, 2003.
39. Ramiasa, M.; Ralston, J.; Fetzer, R.; Sedev, R. Contact Line Friction in Liquid-Liquid Displacement on Hydrophobic Surfaces. *Journal of Physical Chemistry C* **2011,** *115* (50), 24975-24986.
40. Chremos, A.; Glynos, E.; Koutsos, V.; Camp, P. J. Adsorption and self-assembly of linear polymers on surfaces: a computer simulation study. *Soft Matter* **2009,** *5* (3), 637-645.
41. Cosgrove, T.; Fleer, G. J.; Stuart, M. A. C.; Scheutjens, J. M. H. M.; Vincent., B. *Polymers at Interfaces*; Chapman and Hall: London 1993.
42. Galliano, A.; Bistac, S.; Schultz, J. Adhesion and friction of PDMS networks: molecular weight effects. *J Colloid Interf Sci* **2003,** *265*, 372-379.
43. Braithwaite, G. J. C.; Howe, A.; Luckham, P. F. Interactions between Poly(ethylene oxide) Layers Adsorbed to Glass Surfaces Probed by Using a Modified Atomic Force Microscope. *Langmuir* **1996,** *12* (17), 4224-4237.
44. Fu, Z.; Santore, M. M. Poly(ethylene oxide) adsorption onto chemically etched silicates by Brewster angle reflectivity. *Colloids and Surfaces A: Physicochemical and Engineering Aspects* **1998,** *135* (1–3), 63-75.
45. J. C. Braithwaite, G.; F. Luckham, P. Effect of molecular weight on the interactions between poly(ethylene oxide) layers adsorbed to glass surfaces. *Journal of the Chemical Society, Faraday Transactions* **1997,** *93* (7), 1409-1415.
46. Kalloudis, M.; Glynos, E.; Pispas, S.; Walker, J.; Koutsos, V. Thin Films of Poly(isoprene-b-ethylene Oxide) Diblock Copolymers on Mica: An Atomic Force Microscopy Study. *Langmuir* **2013,** *29* (7), 2339-2349.

47. Semenov, A. N.; Joanny, J.-F. Structure of Adsorbed Polymer Layers: Loops and Tails. *EPL (Europhysics Letters)* **1995,** *29* (4), 279-284.
48. Jones, R. L.; Spontak, R. J. Effect of chain length and surface density on looped polymers grafted to an impenetrable surface. *The Journal of Chemical Physics* **1995,** *103* (12), 5137-5143.
49. Deruelle, M.; Leger, L.; Tirrell, M. Adhesion at the Solid-Elastomer Interface: Influence of the Interfacial Chains. *Macromolecules* **1995,** *28* (22), 7419-7428.
50. Deruelle, M.; Tirrell, M.; Marciano, Y.; Hervet, H.; Leger, L. Adhesion energy between polymer networks and solid surfaces modified by polymer attachment. *Faraday Discussions* **1994,** *98* (0), 55-65.
51. Cohen, C.; Restagno, F.; Poulard, C.; Leger, L. Incidence of the molecular organization on friction at soft polymer interfaces. *Soft Matter* **2011,** *7* (18), 8535-8541.
52. Léger, L.; Raphaël, E.; Hervet, H. Surface-Anchored Polymer Chains: Their Role in Adhesion and Friction. In *Polymers in Confined Environments*, Granick, S., Ed.; Springer Berlin Heidelberg, 1999; Vol. 138, pp 185-225.
53. Bureau, L.; Léger, L. Sliding Friction at a Rubber/Brush Interface. *Langmuir* **2004,** *20* (11), 4523-4529.
54. Léger, L.; Creton, C. Adhesion mechanisms at soft polymer interfaces. *Philosophical Transactions of the Royal Society A: Mathematical, Physical and Engineering Sciences* **2008,** *366* (1869), 1425-1442.
55. Léger, L.; Hervet, H.; Charitat, T.; Koutsos, V. The stick–slip transition in highly entangled poly(styrene-butadiene) melts. *Advances in Colloid and Interface Science* **2001,** *94* (1–3), 39-52.

ToC graphic